HHS Public Access

Author manuscript

Physiol Meas. Author manuscript; available in PMC 2014 September 04.

Published in final edited form as:

Physiol Meas. 2013 December ; 34(12): 1593–1609. doi:10.1088/0967-3334/34/12/1593.

Development of a transportable neutron activation analysis system to quantify manganese in bone *in vivo*: feasibility and methodology

Yingzi Liu[1], **David Koltick**[2], **Patrick Byrne**[1,3], **Haoyu Wang**[2], **Wei Zheng**[1], and **Linda H Nie**[1]

Linda H Nie: hnie@purdue.edu

[1]School of Health Sciences, Purdue University, West Lafayette, IN, USA

[2]Physics Department, Purdue University, West Lafayette, IN, USA

[3]Medical Physics Consultants, Inc. Indianapolis, IN, USA

Abstract

This study was conducted to investigate the methodology and feasibility of developing a transportable neutron activation analysis (NAA) system to quantify manganese (Mn) in bone using a portable deuterium–deuterium (DD) neutron generator as the neutron source. Since a DD neutron generator was not available in our laboratory, a deuterium–tritium (DT) neutron generator was used to obtain experimental data and validate the results from Monte Carlo (MC) simulations. After validation, MC simulations using a DD generator as the neutron source were then conducted. Different types of moderators and reflectors were simulated, and the optimal thicknesses for the moderator and reflector were determined. To estimate the detection limit (DL) of the system, and to observe the interference of the magnesium (Mg) γ line at 844 keV to the Mn γ line at 847 keV, three hand phantoms with Mn concentrations of 30 parts per million (ppm), 150 ppm, and 500 ppm were made and irradiated by the DT generator system. The Mn signals in these phantoms were then measured using a 50% high-efficiency high-purity germanium (HPGe) detector. The DL was calculated to be about 4.4 ppm for the chosen irradiation, decay, and measurement time. This was calculated to be equivalent to a DL of about 3.3 ppm for the DD generator system. To achieve this DL with one 50% high-efficiency HPGe detector, the dose to the hand was simulated to be about 37 mSv, with the total body equivalent dose being about 23μSv. In conclusion, it is feasible to develop a transportable NAA system to quantify Mn in bone *in vivo* with an acceptable radiation exposure to the subject.

Keywords

IVNAA; DD neutron generator; Mn; hand bone

The authors report no conflicts of interest.

1. Introduction

Manganese (Mn) is an essential element to human health. However, overexposure to Mn or Mn-containing compounds can lead to adverse health effects. Occupational and environmental exposure to Mn has been associated with kidney and liver disease (Chetri and Choudhuri 2003), cardiovascular disorders (Jiang and Zheng 2005), and, most significantly, neurological disorders (Rodier 1955, Sassine et al 2002, Wennberg et al 1991). In its final stage, Mn toxicity manifests along with a psychological disorder termed manganism, with signs and symptoms that closely resemble Parkinson's disease (Goldhaber 2003, Martin 2006, Santamaria et al 2007). Mn exposure occurs mainly through occupational routes, such as manufacturing and welding (Wang et al 1989). Environmental exposure to Mn, such as through the combustion of Mn-containing gasoline available in the US and several other countries (Butcher 2002), as well as high Mn levels present in diet and drinking water (Bouchard et al 2011), has lately been receiving increasing public attention. An important aspect of Mn toxicity is that the progression of the disease continues even after Mn exposure ceases (Bowman et al 2011).

Traditionally, Mn levels in the human body have been estimated from blood, serum, or urine. Cumulative evidence, however, suggests that there is only a limited relationship between Mn exposure and the concentration of Mn in these biological samples (Crossgrove and Zheng 2004, Smith et al 2007, Zheng et al 2000). Recently, T_1-weighted MRI image technology has been developed to assess Mn exposure using the signal intensity in the basal ganglia region of the brain (Dydak et al 2011, Jiang et al 2007, Qin et al 2009). While it is advantageous to directly relate Mn exposure to brain function, this technology is limited in that the Mn signal reflects only recent Mn exposure. To overcome these technical limitations in accurately measuring Mn exposure, there is a need to develop a noninvasive method for reliable assessment of the body's Mn burden.

There have been some studies on Mn concentrations in animal bone (Dorman et al 2005, Seaborn and Nielsen 2002); however, only a few papers have reported on Mn in human bone specifically (Andersen et al 1999, Pejovic-Milic et al 2009, Schroeder et al 1966). Schroeder et al (1966) reported an average concentration of 2 mg of Mn per kg of bone ash. Taking into account a factor of 1.67 and 1.78 between the weight of bone ash and wet bone for cortical and trabecular bones (Gong et al 1964), a percentage of 80% and 20% of cortical and trabecular bone in human body, as well as an average of 5500 g of wet bone in a reference human male (ICRP 2002), the total Mn in bone ash was calculated to be about 6.5 mg. Given the total body burden of Mn of about 20 mg (Schroeder et al 1966), it is reasonable to suggest that about 32.5% of body Mn is stored in bone. Indeed, Andersen et al (1999) reported 40% of body Mn in bone.

There are no data on the retention rate of Mn in human bone. Animal studies have shown a much longer retention time for Mn in bone than in other tissues and organs. For instance, one study of the clearance rate of Mn in primates showed a relatively long retention half-life of around 220 days from the head, indicating a long half-life in skull because the biological half-life of Mn in brain tissue is much shorter (Newland et al 1987). Data in the literature also show that Mn in rat bone has a prolonged half-life ($t_{1/2}$) of more than 50 days (Furchner

et al 1966, Scheuhammer and Cherian 1983), which is much longer than that of other rat tissues. Thus, it is logical to postulate that bone is one of the main storage organs for Mn, and that Mn remains present in bone long after exposure ceases. Hence, it is desirable to develop an acceptably sensitive technology that can accurately quantify the Mn present in bone and enable use as a measure of exposure.

In vivo neutron activation analysis (IVNAA) is a promising technique that allows for the noninvasive quantification of concentrations of various elements in the human body. Whole body and partial body IVNAA technologies have been used for *in vivo* element analysis for over three decades (for example, Chettle and Fremlin 1984, McNeill et al 1973, Spinks et al 1980) and has made notable contributions to recognizing the association between toxic metals and various health outcomes (Davis et al 2008, Ellis et al 1984, Lewis et al 1997, Mason et al 1988). IVNAA is highly sensitive and capable of quantifying multiple elements at the same time. Currently, the only operating IVNAA system available with the potential for bone Mn assessment for human health studies exists at McMaster University in Canada (Aslam et al 2008, Pejovic-Milic et al 2009). This system, however, is a laboratory accelerator-based NAA system and requires a Tandetron accelerator, and a large laboratory space. For these reasons, it is not practical for this system to be transported to a place where it is mostly needed, such as a factory or a hospital.

In this project, we investigated the feasibility of developing a transportable IVNAA system for bone Mn quantification using a portable deuterium-deuterium (DD) neutron generator as the neutron source, where the reaction $D+D \rightarrow n+{}^{3}He$ produces 2.45 MeV mono-energetic neutrons. Because a DD neutron generator was not available in our laboratory, a deuterium-tritium (DT) neutron generator coupled with a uranium block was used to obtain experimental data. The uranium block served as a neutron amplifier/moderator to amplify the neutrons and shift the neutron energy. Monte Carlo (MC) simulations were performed for both a DD generator system setup as well as the DT generator system setup. The experimental data from the DT generator system setup were used to validate the MC simulation results for the DD generator system and to estimate the detection limit (DL) of the DD system. The overall feasibility of the DD generator system setup was assessed based on the MC simulation results and the results from the DT generator system.

The hand, in theory, would be the most practical place for real human subjects to have their bone Mn measurements taken with IVNAA technology. Targeting bone in the hand would allow the bodily radiation dose from the neutron field to be kept at a minimum, as the hand can be extended far from the body's core and can be shielded in an arm-reach cavity so that the rest of the body receives minimal radiation. Therefore, for this study, testing was carried out on phantoms that represented the bone and flesh of human hands.

2. Material and methods

2.1. Neutron activation analysis

During neutron activation, characteristic γ-rays are produced following the radioactive decay of the product from an ${}^{A}X(n,\gamma)^{(A+1)}X$ nuclear reaction. The energy of the delayed γ-ray is specific to each specific element. For Mn, characteristic γ-rays are produced through

a ^{55}Mn(n, γ)^{56}Mn reaction. ^{55}Mn has a natural abundance of 100% and a relatively high thermal neutron capture cross-section of 13.3 barns. ^{56}Mn decays by beta emission followed by the emission of an 847 keV γ-ray (branch ratio 100%). The ^{56}Mn line has a half-life of 2.58 h, allowing for delayed γ-counting.

The sensitivity DL of the system relies on the intensity of the 0.847 MeV γ-rays produced by the interaction, which is calculated as:

$$A=\frac{6.02\times10^{23}\cdot W\cdot\theta\cdot\phi\cdot\sigma\cdot\gamma\cdot\varepsilon\cdot S\cdot D\cdot C}{M} \quad (1)$$

where A is the activity of the element after irradiation; W is the mass of the element in mg; M is the atom mass for the element in mg mol^{-1}; θ is the abundance of the isotope in the element before irradiation; φ is the neutron flux; σ is the cross-section of the reaction; γ is the branch ratio of the γ-rays; ε is the absolute detection efficiency; S is the saturation factor; D is the decay factor; and C is the counting factor. From the formula, the intensity of the γ-rays is proportional to the concentration of the element, the abundance of the activation isotope, the thermal neutron cross-section, and the neutron flux. The intensity of the γ-rays is also affected by irradiation, delay, and measurement time. The process of system design in this study used MC simulations to optimize these factors and to obtain maximum activation with minimum radiation dose exposure.

2.2. DD neutron generator, DT neutron generator, and uranium moderator

DD and DT neutron generators are small accelerators that emit mono-energetic neutrons characterized by the type of nuclear reaction exploited in each generator. These nuclear reactions are commonly known as DD and DT reactions, and are given by:

$$d+d\rightarrow{}^{3}\mathrm{He}+n$$
$$d+t\rightarrow{}^{4}\mathrm{He}+n.$$

The DD reaction has a Q-value of 3.3 MeV and emits neutrons with energy of about 2.45 MeV. The DT reaction has a Q-value of 17.6 MeV and emits neutrons with energy of about 14.1 MeV.

Neutron generators utilize these reactions by creating ions of DT, and accelerating these ions into a metal hydride loaded with DT. The DD neutron generator used in this study's MC simulations is a model DD-108 generator manufactured by Adelphi (Adelphi Technology, Inc., Redwood, CA). A simplified structure of the DD generator head is shown in figure 1.

The deuterium ion pairs are produced by an ion source within the generator. The ions are accelerated by high voltage of 80–120 keV onto a V-shaped copper target coated with hydrogenated titanium, with the hydrogen replaced by deuterium. For biological assessment, the sample (in this case, the phantom hand) is placed at the side of the V-shaped target to allow it to come into contact with the highest neutron flux.

The DT neutron generator used for the MC simulations and the experiments in this study was the model A-325 manufactured by ThermoFisher Scientific (Thermo Fisher Scientific Inc., Waltham, MA 02454). The target for this generator is a copper-backed zirconium tritide film and contains about 110 GBq of tritium. The formation of the DT generator head is similar to that of the DD generator head, except that the structure of the target is different.

For our application, a DD generator-based system has several advantages over the DT system: (1) a DD generator-based system is more portable as compared to a DT generator-based system; (2) it is much easier to shield a DD generator based-system than to shield a DT generator-based system; (3) DD generator does not contain radioactive material as DT does, so there are less issues to consider in terms of radiation contamination and licensing; (3) there is no interference of the Mn γ-ray peak from the interaction ^{56}Fe(n, p)^{56}Mn, which has a threshold of 4 MeV; and (4) the inelastic neutron scattering cross-sections in carbon and oxygen are much lower when the neutron energy is 2.45 MeV (as with a DD generator) as compared to 14.1 MeV (as with a DT generator); this would significantly decrease the background of the γ-ray spectrum, as materials containing carbon and oxygen are commonly used in shielding and moderating.

Because we only had access to a DT neutron generator for this feasibility study, we shifted the neutron energy using a uranium block for a neutron moderator/amplifier. The uranium block used in this study was a 340.2 kg hollow semi-cylindrical block (38.7 cm diameter × 37.5 cm height) with an inner radius of 5.1 cm in which the DT neutron generator was placed. Figure 2 shows a schematic plot of the uranium block. According to the work performed by the group of one of our co-authors (DK), the neutron energy shifted to lower side with the number of reflected neutrons maximized at approximately 1 MeV by using this uranium block (McConchie 2007, Page 78, Figure 4.8).

2.3. Monte Carlo simulations

MC simulation is a powerful tool to simulate radiation transportation. The MC N-Particle (MCNP) transport code version 5, developed by the researchers at Los Alamos National Laboratory (http://mcnp.lanl.gov/, accessed Sept.13, 2013), has been used in this project. The DT source was simulated as a point source because the target surface was very small ($\sim$1 cm^2). The DD source was simulated as a surface source, with the area set to be the same as the target surface. The generator heads and their neutron emissions were constructed as per the dimensions provided by the manufacturer. The hand was modeled as a sandwich of 9 × 18 cm^2 dimensions consisting of a 0.835 cm thickness of bone between two layers of 0.5 cm thickness of soft tissue. The hand bone compositions used in the MC simulation was obtained from ICRP23 (ICRP 1975). The S (α,β) thermal neutron treatment model was not applied in the simulations.

2.4. Mn-doped hand phantoms

To estimate the DL of the system with experiments, three Mn-doped hand phantoms were made. Since 95% of human bone consists of cortical bone, the concentration of each element in the hand was calculated based on ICRP23's (ICRP 1975) gross and element content of the cortical bone of a reference human male. Only the elements that contribute to the NAA (i.e.,

Ca, Cl, Mg, Na, and Mn) were added to the phantoms. Each of the three hand phantoms had Mn concentrations of about 30, 150, and 500 parts per million (ppm), respectively. The mass of each element and compound used is listed in table 1.

Importantly, human bone has a much higher concentration of magnesium (Mg) than Mn. As shown in table 1, the NAA reactions for Mg and Mn are ^{26}Mg(n, γ)^{27}Mg and ^{55}Mn(n, γ)^{56}Mn. The energy for the ^{27}Mg γ line is 844 keV, which is very close to the energy for the ^{56}Mn γ line, which is 847 keV. Although ^{26}Mg has a much lower isotopic abundance and a much lower thermal neutron capture cross-section than ^{55}Mn, the amount of Mg presented in bone may still cause interference to the Mn γ-ray peak. To observe the interference of Mg in terms of accurately detecting Mn concentration in bone, 50 times more Mg than would be present in a natural hand was added to be attached to the 30 ppm Mn phantom hand. So, the Mg interference observed in the 30 ppm Mn phantom hand would represent the amplitude of the Mg interference that would occur for a hand with 0.6 ppm Mn and the normal amount of Mg. As the concentration of Mn in bone for the average person is about 1 ppm, 0.6 ppm Mn and a normal amount of Mg in the hand are reasonable numbers to address the interference issue. Measurements for the phantoms were also made at three different decay times to test how to best reduce the interference of Mg by changing the decay and measurement time since ^{27}Mg has a much shorter half-life than ^{56}Mn (i.e., 9.45 min versus 2.58 h, respectively).

2.5. HPGe γ-ray detector systems

To measure the Mn characteristic γ-rays produced through the experiment with the DT neutron generator, two types of high-purity germanium (HPGe) systems were used in this study. By the time of the validation study (section 3.1.), only a low-efficiency HPGe detection system was available. It is a Tennelec model 950 HPGe detector attached to a 30 l liquid nitrogen dewar (ORTEC, Oak Ridge, Tennessee). A lead housing was built around the detector system to lower the background counts. DSPEC plus digital signal processing box and Maestro γ-ray spectroscopy software were used for signal collection (ORTEC, Oak Ridge, Tennessee). The detector had an absolute efficiency of 0.75% on the surface of the detector for the 847 keV γ-rays.

For the experiments with the hand phantoms, a high-efficiency HPGe detector was used. It is an model GMX504P HPGe detector with an electromechanical cooler (Ortec, Oak Ridge, Tennessee). Again a simple lead housing was built around the detector. The same electronic system and gamma spectrometer described above were applied for this system. The system had a relative efficiency of 50% compared to 3 inch by 3 inch (or 7.62 cm × 7.62 cm) NaI (sodium iodide) detector using a ^{60}Co source of known intensity 25 cm from the surface of the detector. The absolute efficiency for the system was measured to be 11% at 15 cm away from the source for the 847 keV γ-rays.

2.6. Experimental setup with the DT neutron generator

The first part of the experiments using the DT neutron generator was intended to validate the MC simulation results. Samples of $MnCl_2.4H_2O$, which contained either 0.442 g or 0.486 g of Mn, were placed in plastic vials under the depleted uranium block. The samples were then

irradiated at one of two settings. In the first configuration, depleted uranium (DU) was used as a moderator and neutron multiplier, while there was no paraffin wax (will be referred to as paraffin hereafter) present. In the second configuration, paraffin was placed under the Uranium block and the sample to act as a reflector, as to backscatter neutrons.

For the second part of the experiments where the three hand phantoms were irradiated, the phantoms were placed in between two layers of paraffin. The thickness of the top layer is 5 cm, and the thickness of the bottom layer is 10 cm. The setup of the irradiation system used for the second configuration for the first part of the experiments is shown in figure 3. The settings for the other experiments were similar except the different arrangements of the paraffin blocks.

3. Results

3.1. Simulation results using the DT generator for validation

In our experiment, the plastic vials containing $MnCl_2 \cdot 4H_2O$ were irradiated for 10 min. After 40 min' cooling, the samples were measured using the HPGe detector for 10 min. In the first configuration with the DT neutron generator, where no paraffin was used as a reflector, the maximum neutron fluence was at 0.7 MeV, and there was no neutron fluence at energies less than 1 keV. The neutron fluence spectrum as a function of neutron energy is illustrated in figure 4.

Figure 5 shows the MC simulation results for the neutron energy distribution of the second configuration, where 10 cm of paraffin was placed under the DU moderator and the samples were placed between the DU moderator and the paraffin reflector. By applying the paraffin reflector, there was a strong thermal neutron fluence between the energy ranges from 3.98×10^{-9} to 2×10^{-7} MeV. The Mn neutron capture cross-sections in this energy range spanned from 7.5 to 98.0 barns. The neutron capture rate was significantly enhanced due to the presence of the paraffin.

The Mn line count rates obtained from the detector were 0.99 ± 0.04 and 1.13 ± 0.04 counts per second for the 0.442 and 0.486 g Mn samples, respectively, in the irradiations where the paraffin was present. Based on the MC simulation results for activated atoms and calculations using equation (1), however, the expected Mn line count rates were estimated to be 0.84 and 0.94 counts per second, respectively. The difference between the counts calculated from the MC simulations and those obtained from the experiments using the DT generator system setup could have resulted from: (1) slightly different source definitions and generator configurations; or (2) a small variance in irradiation time, which began to be recorded when the neutron emission rate increased to 3×10^8 neutrons per second. It took around 1 min for the neutron generator to reach this value from 0, and another minute of irradiation was added to the sample when we scaled down the neutron emission rate from 3×10^8 neutrons per second to 0 after 10 min of irradiation. Therefore, more activated ^{56}Mn atoms were present in the experiment than were calculated from the MC simulations. Nonetheless, the approximate agreement between these results is promising in terms of MC simulations using a DD generator being able to give reliable predictions of the feasibility of quantifying Mn in bone in the hand.

3.2. The Mn spectrum, Mg interference, and the detection limit

Hand phantoms containing 30, 150, and 500 ppm Mn were irradiated using the DT generator. Three measurements were made for each phantom using the 50% high-efficiency HPGe to observe Mg interference and to determine the DL of the technology. The first measurement was made 5 min after the irradiation, and the measurement was taken over a 10 min span. The second measurement was taken immediately following the first measurement, and was taken over 20 min. The third measurement was taken immediately following the second measurement, and was taken over 40 min.

Figure 6(a) shows the spectrum for the first measurement of the 30 ppm Mn-doped phantom at an energy range of 830–860 keV. Both the Mn and Mg peaks were clearly visible at the time of the first measurement. Figure 6(b) shows the spectrum for the third measurement for the 30 ppm Mn phantom; here, only the Mn is visible because, as previously mentioned, ^{27}Mg has a much shorter half-life than ^{56}Mn (i.e., 9.45 min versus 2.58 h), and hence the ^{27}Mg had already decayed. These figures suggest two important conclusions: (1) that the Mg peak is clearly distinguishable from the Mn peak when using HPGe detectors, so there is no need for concern about Mg interference when using an HPGe detector for γ-ray detection; and (2) even if a detector system with a worse energy resolution is used (e.g., an NaI detector system), Mg interference can still be eliminated by allowing for sufficient decay time between irradiating the sample and taking measurements, without significant loss of the Mn signal.

The DL of the system was calculated based on the measurements taken from the 30 ppm Mn phantom. It was calculated using the following formula:

$$\mathrm{DL}=\frac{2\times\sqrt{\mathrm{background}}}{C} \quad (2)$$

where background is the background counts under the Mn γ-ray peak, and C (counts/ppm) was calculated using the net count under the Mn γ-ray peak divided by the concentration of the phantom. The energy range of the background was estimated as 4 sigma of the Mn γ-ray Gaussian peak, which covers 96% of the peak counts. The energy range of was 841.6–852.4 keV. Gamma-ray spectrum analysis was performed using an in-house fitting procedure programmed in the commercial software package IGOR Pro 6 (Wave Metrics, Inc., Lake Oswego, USA), as were the calculations for the sigma of the Mn γ-ray peak and the background of the peak.

To obtain better statistics for the constant C (ppm/count) and to test the reproducibility of the system, we irradiated and measured two other phantoms with concentrations of 150 ppm Mn and 500 ppm Mn. Figure 7 shows the spectrum for the 150 ppm phantom for the third measurement (35 min decay time followed by 40 min of measurement time) at the energy range of 830–860 keV. The net peak counts under the 847 keV γ-ray peak for the 150 ppm Mn phantom and for the 500 ppm Mn phantom for the third measurement (35 min of decay time followed by 40 min of measurement time) were calculated to be 347 ± 20 and 1065 ± 37, respectively. The DLs from the spectra of the 30 ppm phantom for the 10 min

measurement time, 20 min measurement time, and 40 min measurement times were 12.5 ppm, 7.3 ppm, and 4.4 ppm, respectively.

3.3. MC simulation results for the DD generator

Many MC simulations were performed to determine the optimized moderator, reflector, and shielding setup for the DD generator-based system to measure Mn concentrations in human hand bones. Because of energy and momentum conservation, neutron is more likely to lose its energy when it collides with an atom with the same and close mass. Hence, the ideal moderator materials for an IVNAA-based neutron source would have a low atomic number, a large neutron elastic scattering cross-section, and minimum γ-ray production. In this study, 7 cm each of graphite, paraffin, polyethylene, and both light and heavy water were simulated as moderating materials. Paraffin was selected as the best moderator because of its high thermal neutron fluence and low fast neutron fluence. The neutron fluence results were illustrated in figure 8, and corresponding neutron fluence at the 3.98×10^{-3} to 0.2 eV (thereafter refer to as thermal range) and 6.31×10^{4} to 3.16×10^{6} eV (thereafter refer to as fast range) ranges were shown in table 2.

The optimal reflector was determined based on simulations comparing 6 cm layers of lead, graphite, paraffin, aluminum, and polyethylene. The neutron fluence at the thermal energy range and the fast energy range, results combining 7 cm of paraffin as a moderator and 6 cm of the various reflectors were shown in table 3. Paraffin was selected as the best reflector due to its high fluence of thermal neutrons and low fluence of fast neutrons. The setup of the DD neutron generator with paraffin as both a moderator and a reflector is illustrated in figure 9.

The peaks of thermal and fast neutron fluences at different moderator thicknesses were listed in table 4. (The reflector thickness is constant at 6 cm in all these simulations.) It was determined that thermal neutron fluences were highest when the paraffin moderator was at 4 cm and 5 cm thicknesses; however, the fast neutron fluence was higher at 4 cm. Hence, 5 cm was determined to be the optimum thickness for the paraffin moderator.

As shown in figure 10, with the paraffin moderator thickness at 5 cm, when the paraffin reflector was 10 cm or thicker, the neutron fluence at the thermal energy range did not change significantly, so the optimum thickness of the paraffin reflector was determined to be 10 cm.

3.4. Detection limits and dose calculation

The DLs presented in section 3.2 were the DLs for the DT-based system. The DL for the DD-based system was calculated as:

$$\mathrm{DL_{DD}} = \mathrm{DL_{DT}} \times \frac{\mathrm{Mn_{DD}}}{\mathrm{Mn_{DT}}} \quad (3)$$

where $\mathrm{DL_{DT}}$ is the DL determined from the high-efficiency HPGe detector using the DT generator system; $\mathrm{Mn_{DT}}$ is the Mn γ-ray counts determined by MC simulation using the DT-

based system; and Mn_{DD} is the Mn γ-ray counts determined by the MC simulation using the DD-based system. From MC simulations, the optimum DD neutron generator setup has a Mn activation rate that is 2.4 times better than that of the DT setup described in section 3.2. Figure 11 shows the neutron fluences for both the DT and DD setups.

After taking into account the factor of 2.4 and scaling down the neutron flux to make the dose acceptable for *in vivo* study, the DLs calculated for the DD-based system were 9.3, 5.4, and 3.3 ppm for 10-, 20-, and 40 min measurements of neutron flux, respectively, which gives rise to an equivalent hand dose of 37 mSv. These DLs were for 10 min of irradiation time with a neutron flux of 3×10^8 neutrons per second. There are some ways to further improve these DLs, which are considered in the discussion section below.

In the MC simulations, the weighting factors of the neutrons were input according to ICRP60 (ICRP 1991). A high-density polyethylene (HDPE) shielding cavity was constructed as the shield that would need to be used for *in vivo* testing to separate the hand being targeted for direct irradiation from the rest of the body. Through simulations, we determined the optimum thickness for the HDPE box to be 26 cm. Our shielding goal was to ensure that no more than 0.1% of the hand dose was delivered to the rest of the body, and the dose for the rest of the body was calculated to be 19 μSv. Taking into account that approximately 1.25% of the total body skeleton and skin are in the hand (with a tissue weighting factor of 0.01), the whole body effective dose that would be delivered to the subject under these conditions was calculated to be 23 μSv. This is comparable to the amount of radiation delivered by a standard PA chest x-ray (20 μSv) and is negligible comparing to the annual natural background for the general population (3600 μSv in the US (NCRP 1987)).

4. Discussion

In theory, many neutron sources can be used for NAA. However, the number of those that can be used for *in vivo* elemental measurement is quite limited, taking into consideration the dose and cost as well as the portability of the detection system. For instance, ^{252}Cf, which has been used to measure aluminum in bone, is a compact, high-yield fission neutron source (Morgan et al 1990, Wyatt et al 1993); however, with a half-life of 2.65 yr, the source needs to be replaced in a relatively short time. Another disadvantage is that it cannot be turned off, so heavy shielding is required even when the source is not in use. Another neutron source is the accelerator source used by McMaster University (Aslam et al 2008, 2009b). This accelerator system requires a Tandetron accelerator, a big space, and it is not movable as we discussed in the introduction.

In contrast, compact accelerator-based neutron sources such as DD and DT neutron generators operate using charged particles that are accelerated onto a target where neutron-producing reactions occur. Unlike ^{3}H(p,n)^{3}He and ^{7}Li(p,n)^{7}Be reactions, with laboratory thresholds of 1.019 and 1.881 MeV respectively, the neutron-production cross-sections of DD and DT reactions are high at relatively low energies, and an acceleration voltage of around 100 kV is enough to produce high neutron fluences. This makes them viable candidates as portable, compact neutron generators. The advantages of the DT generator are

a long lifespan, lower operating pressure, and high ionization efficiency. However, as discussed above in section 2.1, for our application the DD generator has several vital advantages over the DT generator, including being easier to shield and easier to transport. Since a DD generator was not available in the study lab, the concurrence of the experimental results and the MC simulations of the DT generator was used to validate the simulation outcomes for the DD generator.

The DLs calculated for the 10 min measurement and 40 min measurement with the DT generator setting were 12.5 ppm and 4.4 ppm respectively. With the increase of the measurement time by a factor of 4, an improvement of the DL by a factor of 2 was expected. However, the calculated improvement factor was 2.8 (12.5/4.4). The results indicate that the lower background under the 847 keV peak at longer decay time overcame the limit of the lower Mn γ-ray count rate at longer decay time. In addition, longer decay time will significantly reduce the interference from Mg γ-rays. For these reasons, it is preferable to measure longer at a relatively long decay time. An optimized irradiation, measurement, and decay time will be determined in our future work once a DD generator system is set up in our laboratory.

The best Mn DL as calculated for the DD-based system using a high-efficiency HPGe detector (one detector with a relative efficiency of 50%) was about 3.3 ppm. This DL can be improved in several ways. First, by using an HPGe system with a relative efficiency of 100%, the DL can be reduced to 2.3 ppm. Alternately, by using two HPGe systems each with a relative efficiency of 100%, the DL can be improved to 1.7 ppm. Second, the DL can be improved by a factor of 1.35 if the radiation dose to the hand is increased to 50 mSv. If both factors are combined, a DL of 1.3 ppm can be achieved. Further improvements can be made by optimizing the irradiation, measurement, and decay time as described above. These values are comparable to the ones obtained by the group at McMaster which used the Tandetron accelerator as neutron source (Aslam et al 2009a). The optimized DL reported by them was 0.6 μg Mn g^{-1} Ca with a hand dose of about 74 mSv. As far as we know, this is the only other group who has also been working on the instrumentation development on *in vivo* quantification of Mn in bone.

Because high-efficiency HPGe detectors are very expensive, the use of less expensive NaI detector systems can be explored. One advantage with these NaI systems is that it is easy to build a nearly 4π system, which provides almost 100% absolute efficiency. However, with a resolution that is about 100 times worse than that of the HPGe detector, it is not possible to differentiate the 844 keV Mg peak from the 847 keV Mn peak. However, this problem can be solved with a longer decay time, as illustrated in section 3.2. What's more, there has been progress regarding the NaI(Tl) detection system. Recently, one group developed a 4π γ-ray spectrometer using eight long NaI(Tl) detectors combined with the spectral decomposition method, and further improved the DL as a result of a gain in γ-ray detection efficiency (Byun et al 2006).

Using MC simulations, the neutron dose to the hand after 10 min of irradiation at a neutron flux of 3×10^8 neutrons per second was calculated to be 37 mSv. Currently, there is no standard dose limit for the general public for hand exposure. Considering the many health

risks associated with high Mn exposure, it is reasonable to use the reference annual dose limit for the general public for measuring the Mn present in those subjects exposed to excessive amounts of Mn. According to ICRP60, the annual dose limit to the hand for the general public is 50 mSv. Within this dose range, the risk of irradiation is low and the dose is acceptable. The way to reduce the whole body effective dose is by setting shielding materials between the generator and the rest of the body. With an HDPE box 26 cm thick, the whole body dose is 23 μSv.

5. Conclusion

Experiments and MC simulations for a DT neutron generator were performed to validate the MC simulation results of a DD generator for IVNAA analysis of Mn in bone. The best system design for a DD generator irradiation system was determined from MC simulation results. The detection limit was estimated using a 50% high-efficiency HPGe detector and was calculated to be 3.3 ppm for10 min of irradiation at a neutron flux of 3×10^8 neutrons per second with a DD setup. The dose to the hand was calculated to be 37 mSv, and the total body effective dose was calculated to be 23 μSv when using an HDPE shield. Based on these results, it is feasible to develop a transportable NAA system to quantify Mn in bone *in vivo* with an acceptable radiation dose to the subject.

Acknowledgments

This work was supported by the National Institute for Occupational Safety and Health (NIOSH) R21 grant 1R21OH010044, the NIOSH Pilot Research Project Training Program of the University of Cincinnati Education and Research Center Grant T42/OH008432-06, and the Purdue Faculty Summer Research Grant.

References

Andersen ME, Gearhart JM, Clewell HJ III. Pharmacokinetic data needs to support risk assessments for inhaled and ingested manganese. Neurotoxicology. 1999; 20:161–71. [PubMed: 10385880]

Aslam, Chettle DR, Pejovic-Milic A, Waker AJ. Opportunities to improve the *in vivo* measurement of manganese in human hands. Phys Med Biol. 2009a; 54:17–28. [PubMed: 19060358]

Aslam, Davis K, Pejovic-Milic A, Chettle DR. Noninvasive measurement of aluminium in human bone: preliminary human study and improved system performance. J Inorg Biochem. 2009b; 103:1585–90. [PubMed: 19740544]

Aslam, Pejovic-Milic A, Chettle DR, McNeill FE. Quantification of manganese in human hand bones: a feasibility study. Phys Med Biol. 2008; 53:4081–92. [PubMed: 18782941]

Bouchard MF, et al. Intellectual impairment in school-age children exposed to manganese from drinking water. Environ Health Perspect. 2011; 119:138–43. [PubMed: 20855239]

Bowman AB, Kwakye GF, Hernandez EH, Aschner M. Role of manganese in neurodegenerative diseases. J Trace Elem Med Biol. 2011; 25:191–203. [PubMed: 21963226]

Butcher DJ. Speciation of methylcyclopentadienyl manganese tricarbonyl and its derivatives: a review. Appl Spectors Rev. 2002; 37:1–17.

Byun SH, Pejović-Milić A, Prestwich WV, Chettle DR, McNeill FE. Improvement of in vivo neutron activation analysis of mn using a 4p nai(tl) detector array. J Radioanal Nucl Chem. 2006; 269:615–8.

Chetri K, Choudhuri G. Role of trace elements in hepatic encephalopathy: zinc and manganese. Indian J Gastroenterol. 2003; 22(Suppl 2):S28–S30. [PubMed: 15025250]

Chettle DR, Fremlin JH. Techniques of *in vivo* neutron activation analysis. Phys Med Biol. 1984; 29:1011–43. [PubMed: 6385030]

Crossgrove J, Zheng W. Manganese toxicity upon overexposure. NMR Biomed. 2004; 17:544–53. [PubMed: 15617053]

Davis K, Aslam, Pejovic-Milic A, Chettle DR. *In vivo* measurement of bone aluminum in population living in southern Ontario, Canada. Med Phys. 2008; 35:5115–23. [PubMed: 19070246]

Dorman DC, et al. Maternal-fetal distribution of manganese in the rat following inhalation exposure to manganese sulfate. Neurotoxicology. 2005; 26:625–32. [PubMed: 16112325]

Dydak U, et al. *In vivo* measurement of brain GABA concentrations by magnetic resonance spectroscopy in smelters occupationally exposed to manganese. Environ Health Perspect. 2011; 119:219–24. [PubMed: 20876035]

Ellis KJ, Yuen K, Yasumura S, Cohn SH. Dose-response analysis of cadmium in man: body burden versus kidney dysfunction. Environ Res. 1984; 33:216–26. [PubMed: 6363055]

Furchner JE, Richmond CR, Drake GA. Comparative metabolism of radionuclides in mammals: III. Retention of manganese-54 in the mouse, rat, monkey and dog. Health Phys. 1966; 12:1415–23. [PubMed: 4961684]

Goldhaber SB. Trace element risk assessment: essentiality versus toxicity. Regul Toxicol Pharmacol. 2003; 38:232–42. [PubMed: 14550763]

Gong JK, Arnold JS, Cohn SH. Composition of trabecular and cortical bone. Anat Rec. 1964; 149:325–31. [PubMed: 14208979]

ICRP. Report of the task group on reference man. Ann ICRP. 1975; 3:62–76.

ICRP. Recommendations of the international commission on radiological protection. Ann ICRP. 1991; 21:1–201.

ICRP. ICRP 89: basic anatomical and physiological data for use in radiological protection reference values. Ann ICRP. 2002; 32:1–277.

Jiang Y, Zheng W. Cardiovascular toxicities upon manganese exposure. Cardiovasc Toxicol. 2005; 5:345–54. [PubMed: 16382172]

Jiang Y, et al. Brain magnetic resonance imaging and manganese concentrations in red blood cells of smelting workers: search for biomarkers of manganese exposure. Neurotoxicology. 2007; 28:126–35. [PubMed: 16978697]

Lewis DG, Natto SS, Ryde SJ, Evans CJ. Monte Carlo design study of a moderated 252cf source for *in vivo* neutron activation analysis of aluminium. Phys Med Biol. 1997; 42:625–36. [PubMed: 9127441]

Martin CJ. Manganese neurotoxicity: connecting the dots along the continuum of dysfunction. Neurotoxicology. 2006; 27:347–9. [PubMed: 16337002]

Mason HJ, et al. Relations between liver cadmium, cumulative exposure, and renal function in cadmium alloy workers. Br J Ind Med. 1988; 45:793–802. [PubMed: 3219304]

McConchie, S. Ph D Thesis. Purdue University; 2007. Detection of hazardous materials in vehicles using neutron interrogation techniques.

McNeill KG, Thomas BJ, Sturtridge WC, Harrison JE. *In vivo* neutron activation analysis for calcium in man. J Nucl Med. 1973; 14:502–6. [PubMed: 4351164]

Morgan WD, et al. Development of a technique to measure bone aluminium *in vivo* using a cf-252 neutron source. Basic Life Sci. 1990; 55:437–8. [PubMed: 2088306]

NCRP. report no 93. Bethesda: 1987. NCRP Ionizing radiation exposure of the population of the united states.

Newland MC, Cox C, Hamada R, Oberdorster G, Weiss B. The clearance of manganese chloride in the primate. Fundam Appl Toxicol. 1987; 9:314–28. [PubMed: 3653574]

Pejovic-Milic A, Chettle DR, Oudyk J, Pysklywec MW, Haines T. Bone manganese as a biomarker of manganese exposure: a feasibility study. Am J Ind Med. 2009; 52:742–50. [PubMed: 19753565]

Qin WP, et al. Variations of brain magnetic resonance imaging among manganese-exposed workers. Zhonghua Yu Fang Yi Xue Za Zhi. 2009; 43:793–7. [PubMed: 20137563]

Rodier J. Manganese poisoning in moroccan miners. Br J Ind Med. 1955; 12:21–35. [PubMed: 14351643]

Santamaria AB, Cushing CA, Antonini JM, Finley BL, Mowat FS. State-of-the-science review: does manganese exposure during welding pose a neurological risk. J Toxicol Environ Health B Crit Rev. 2007; 10:417–65. [PubMed: 17710609]

Sassine MP, Mergler D, Bowler R, Hudnell HK. Manganese accentuates adverse mental health effects associated with alcohol use disorders. Biol Psychiatry. 2002; 51:909–21. [PubMed: 12022965]

Scheuhammer AM, Cherian MG. The influence of manganese on the distribution of essential trace elements. Ii. The tissue distribution of manganese, magnesium, zinc, iron, and copper in rats after chronic manganese exposure. J Toxicol Environ Health. 1983; 12:361–70. [PubMed: 6655740]

Schroeder HA, Balassa JJ, Tipton IH. Essential trace metals in man: manganese. A study in homeostasis. J Chronic Dis. 1966; 19:545–71. [PubMed: 5338081]

Seaborn CD, Nielsen FH. Dietary silicon and arginine affect mineral element composition of rat femur and vertebra. Biol Trace Elem Res. 2002; 89:239–50. [PubMed: 12462747]

Smith D, et al. Biomarkers of mn exposure in humans. Am J Ind Med. 2007; 50:801–11. [PubMed: 17924418]

Spinks TJ, Bewley DK, Paolillo M, Vlotides J, Joplin GF, Ranicar AS. Metabolic activity of sodium, measured by neutron activation, in the hands of patients suffering from bone diseases: concise communication. J Nucl Med. 1980; 21:41–46. [PubMed: 7356737]

Wang JD, Huang CC, Hwang YH, Chiang JR, Lin JM, Chen JS. Manganese induced parkinsonism: an outbreak due to an unrepaired ventilation control system in a ferromanganese smelter. Br J Ind Med. 1989; 46:856–9. [PubMed: 2611159]

Wennberg A, Iregren A, Struwe G, Cizinsky G, Hagman M, Johansson L. Manganese exposure in steel smelters a health hazard to the nervous system. Scand J Work Environ Health. 1991; 17:255–62. [PubMed: 1925437]

Wyatt RM, Ryde SJ, Morgan WD, McNeil EA, Hainsworth IR, Williams AJ. The development of a technique to measure bone aluminium content using neutron activation analysis. Physiol Meas. 1993; 14:327–35. [PubMed: 8401272]

Zheng W, Kim H, Zhao Q. Comparative toxicokinetics of manganese chloride and methylcyclopentadienyl manganese tricarbonyl (mmt) in sprague-dawley rats. Toxicol Sci. 2000; 54:295–301. [PubMed: 10774811]

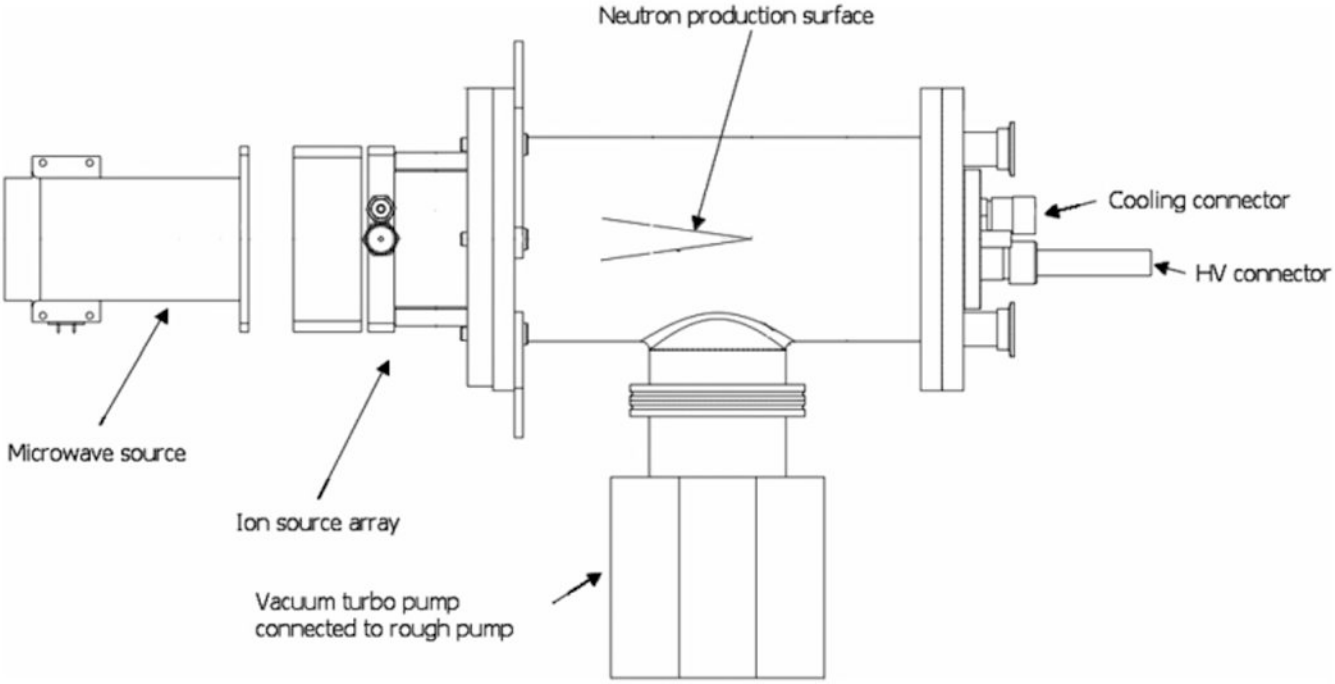

Figure 1.
DD generator head.

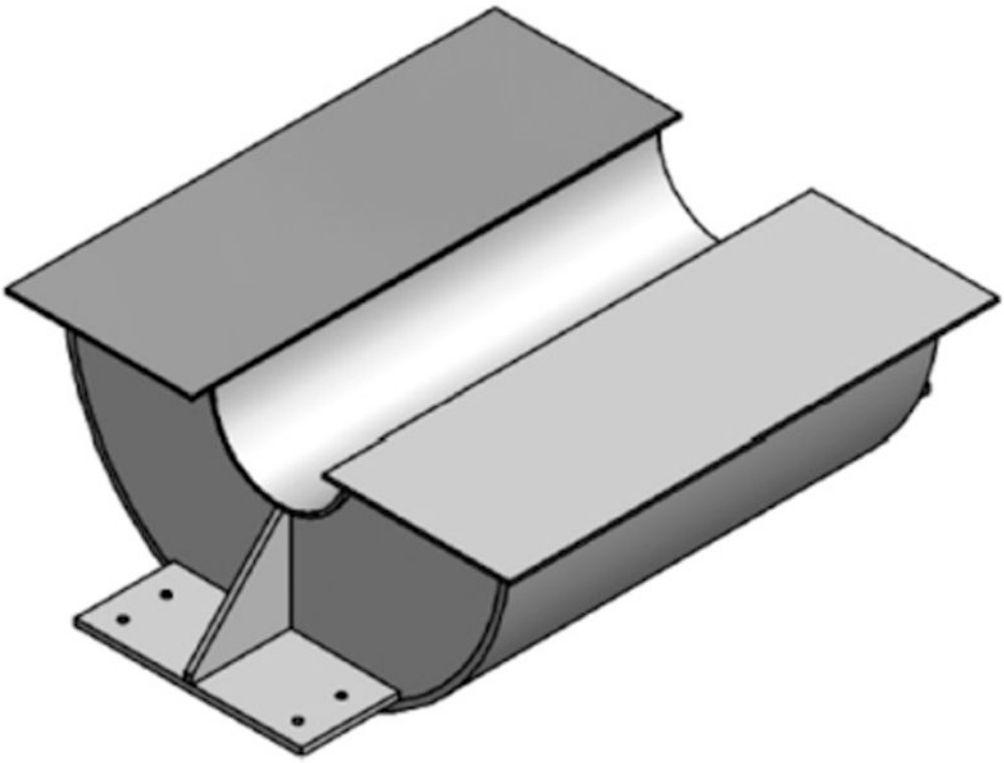

Figure 2.
Uranium block.

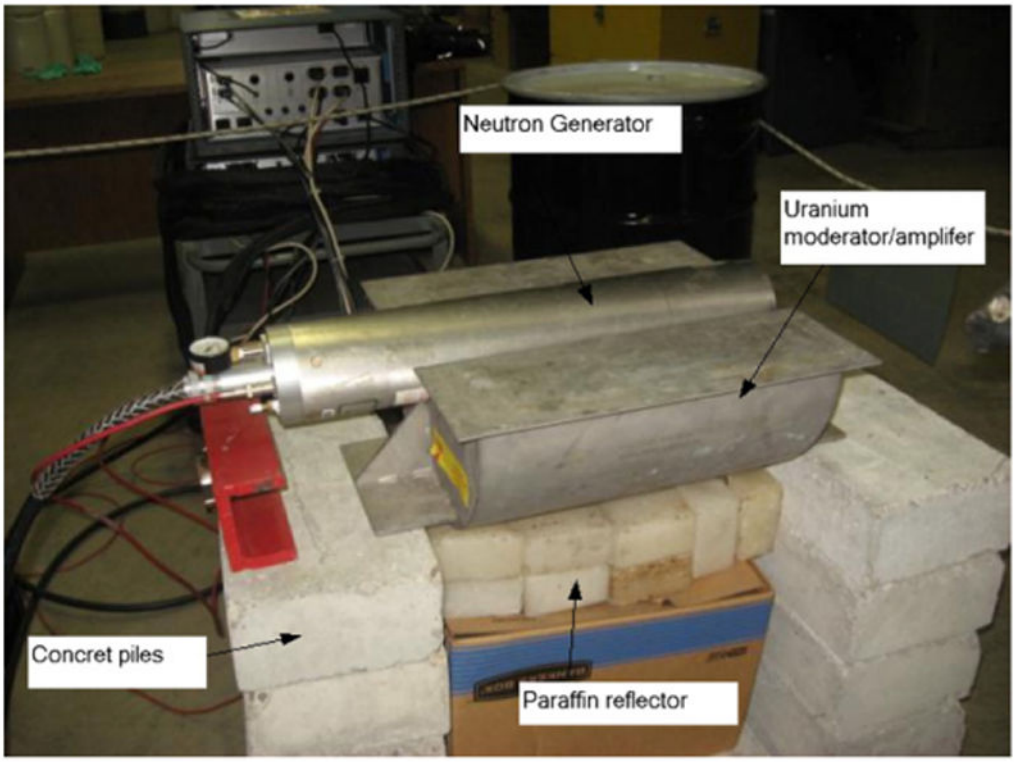

Figure 3.
The setup of the DT irradiation system.

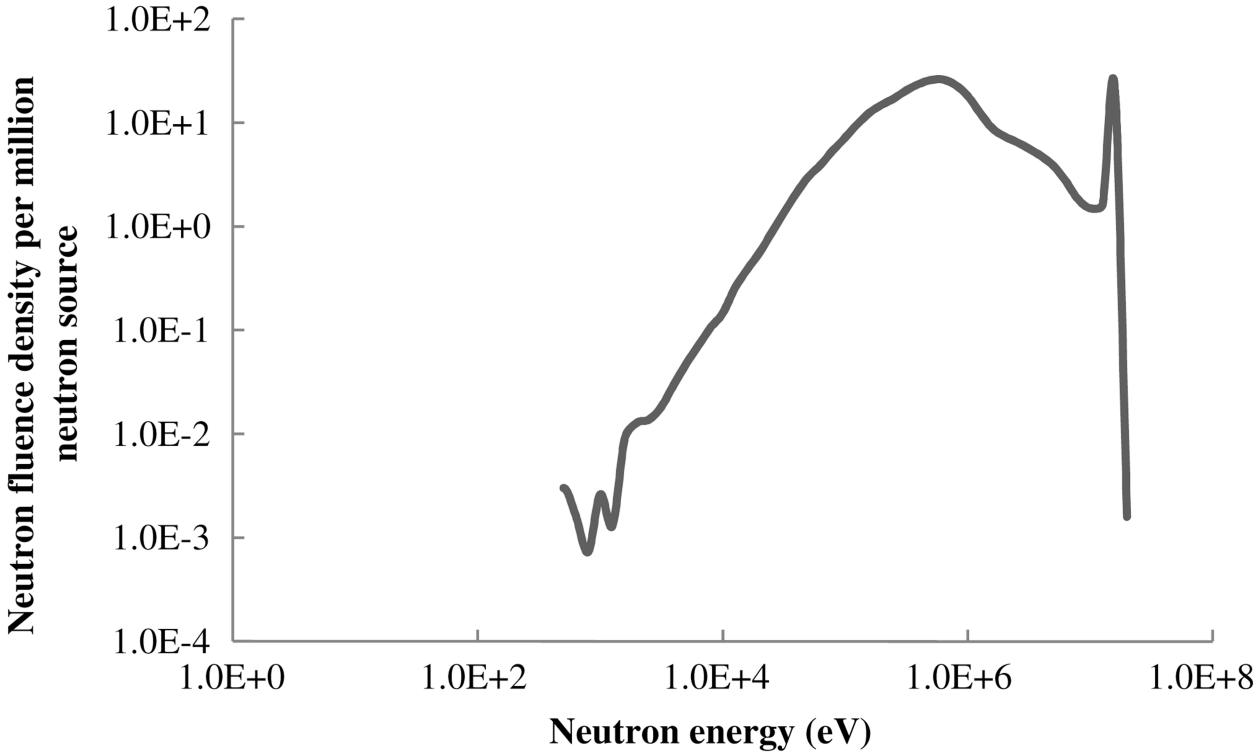

Figure 4.
Neutron energy distribution using depleted uranium as a moderator and amplifier.

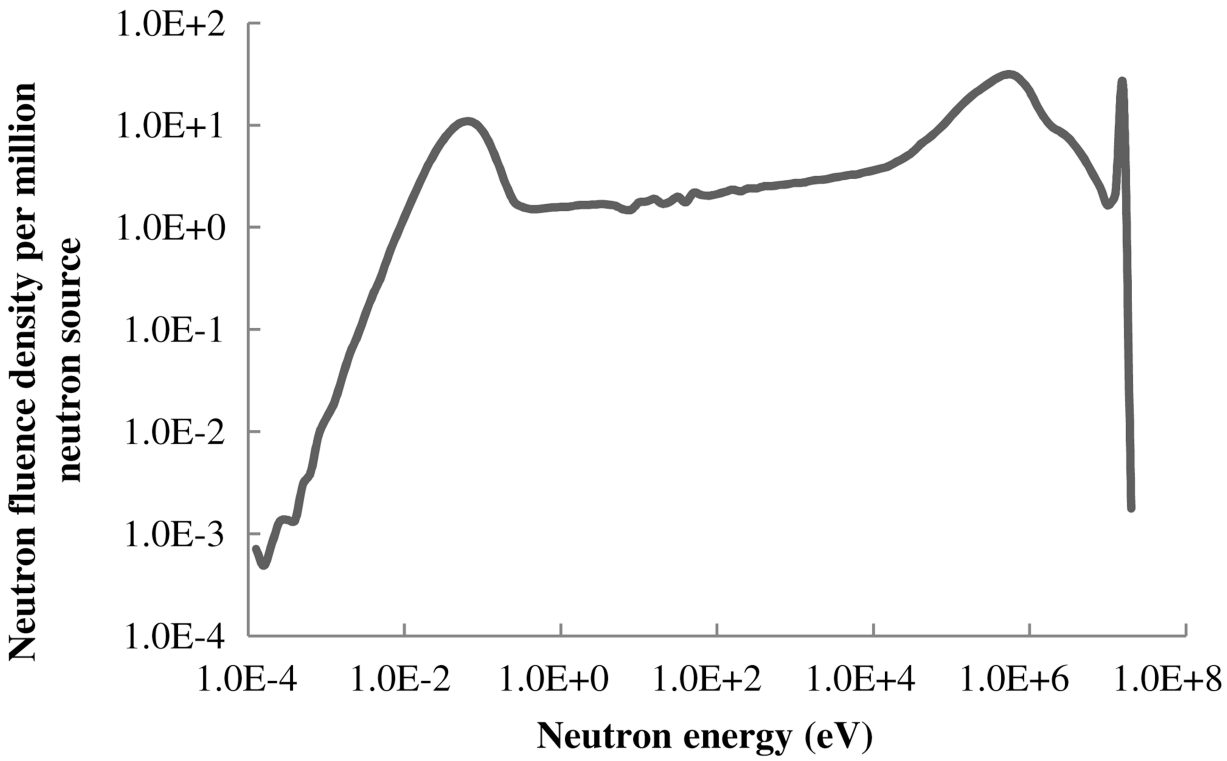

Figure 5.
Neutron energy distribution using depleted uranium as a moderator and amplifier, as well as 10 cm of paraffin as a reflector.

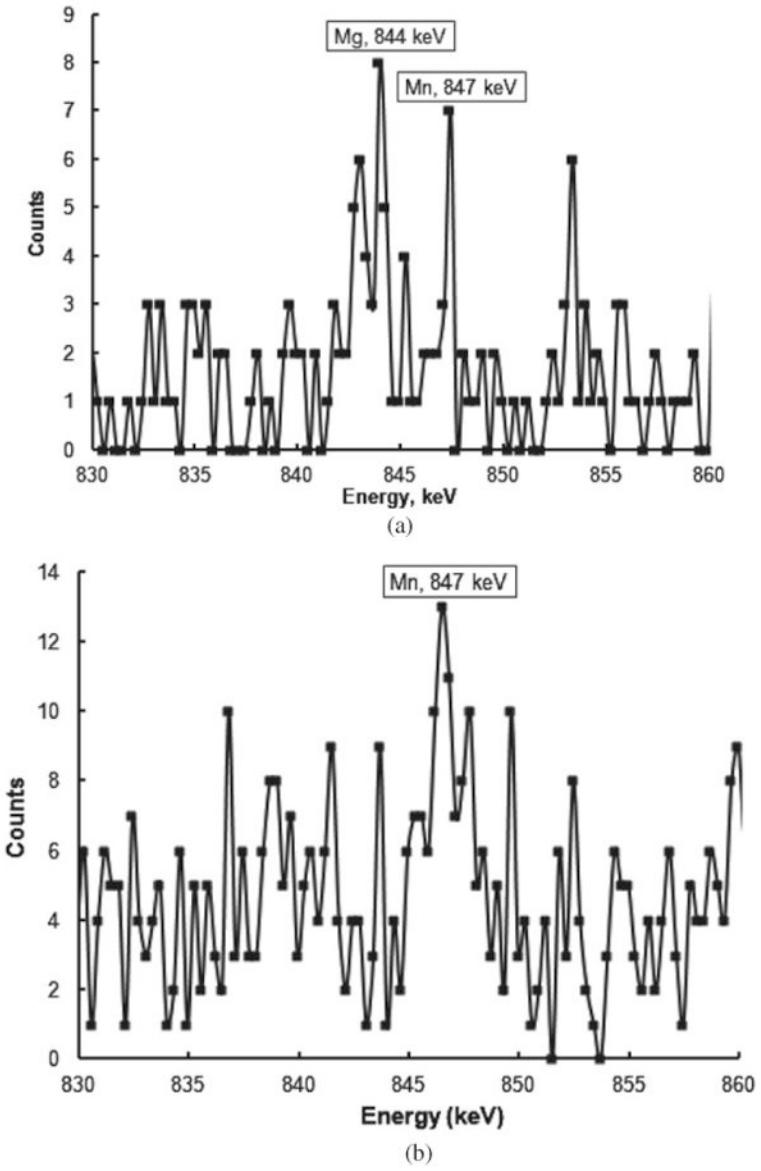

Figure 6.

(a) Spectrum for the 30 ppm Mn phantom (5 min of decay time followed by 10 min of measurement time). (b) Spectrum for the 30 ppm Mn phantom (35 min of decay time followed by 40 min of measurement time).

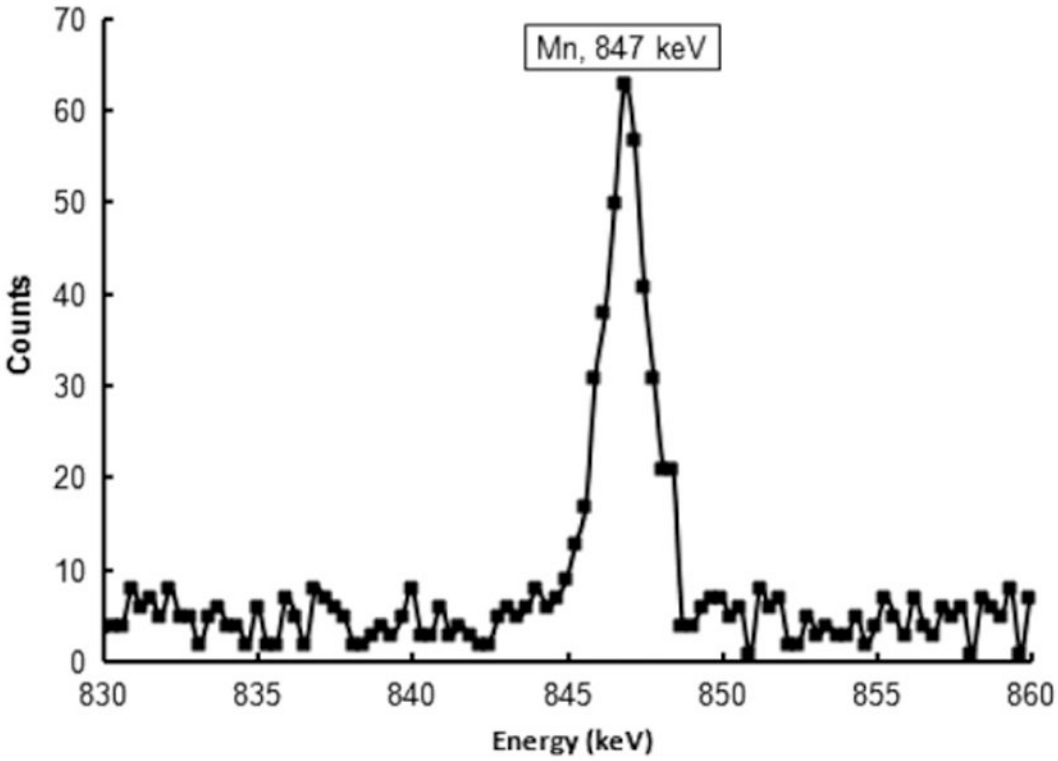

Figure 7.
Spectrum for the 150 ppm Mn phantom (35 min of decay time followed by 40 min of measurement time).

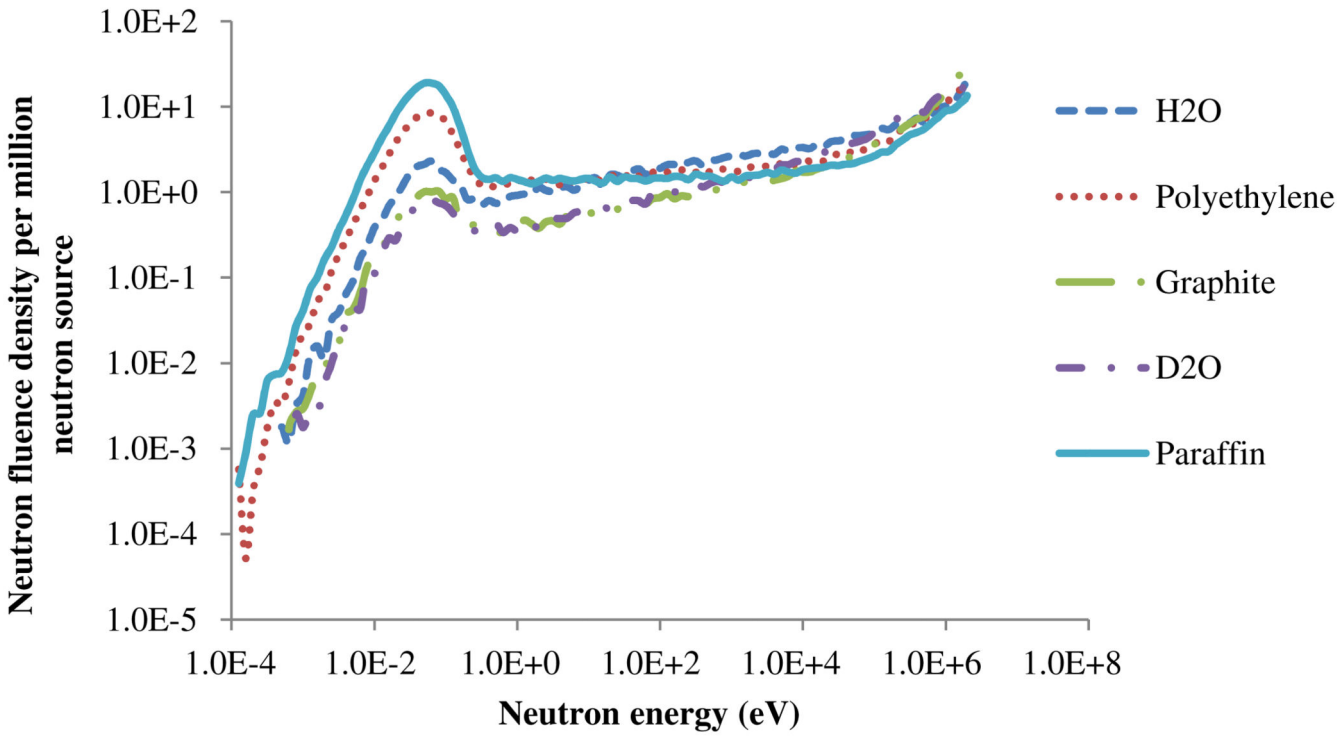

Figure 8.
Neutron fluence spectrum for different moderators, including paraffin.

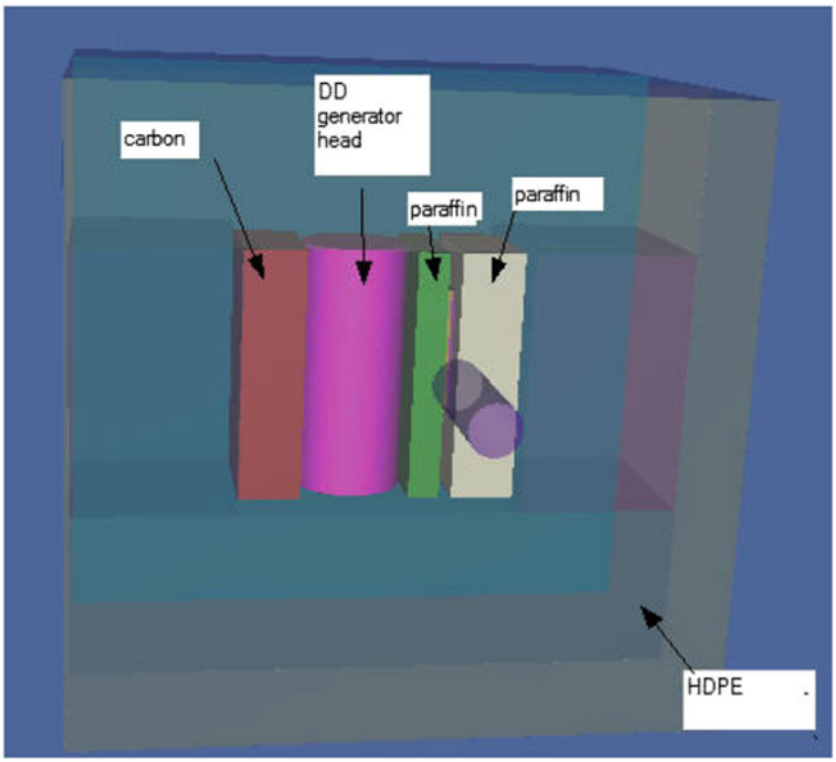

Figure 9.
The setup design of the DD irradiation system.

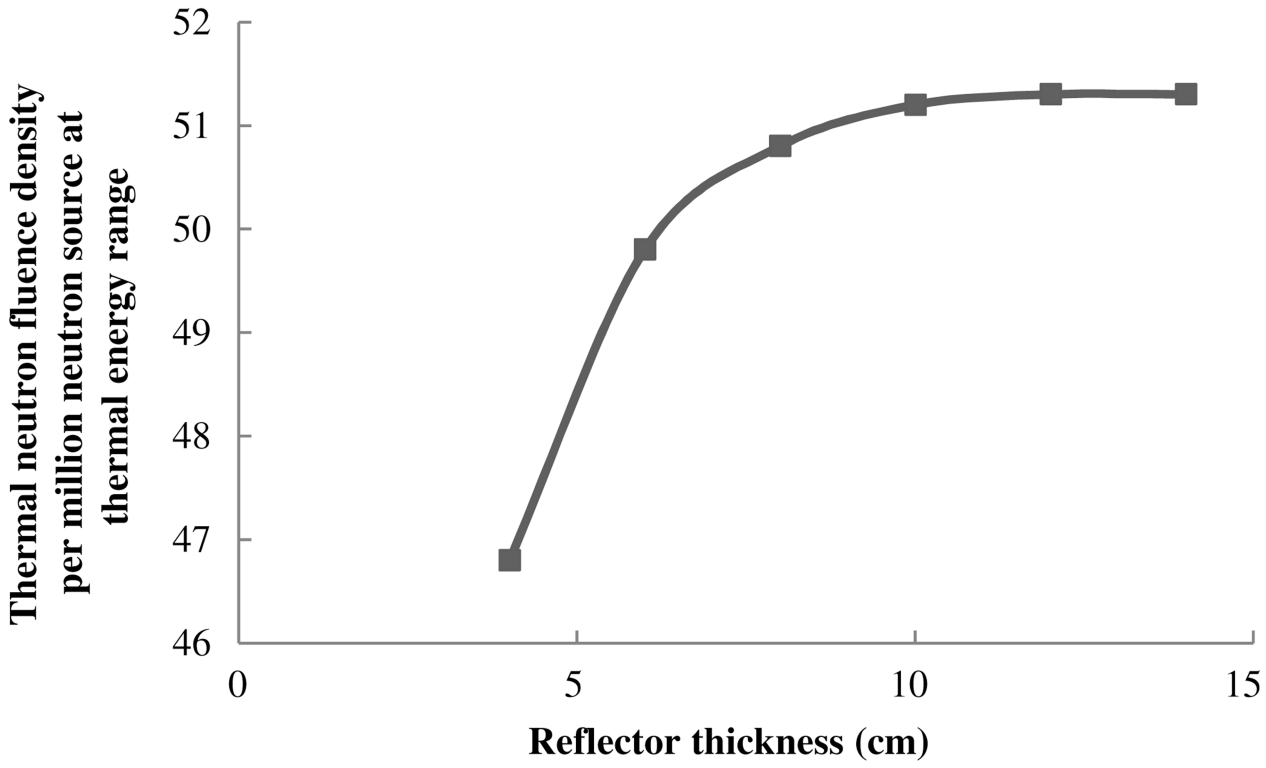

Figure 10.
Different thicknesses of paraffin reflectors with a 5 cm paraffin moderator.

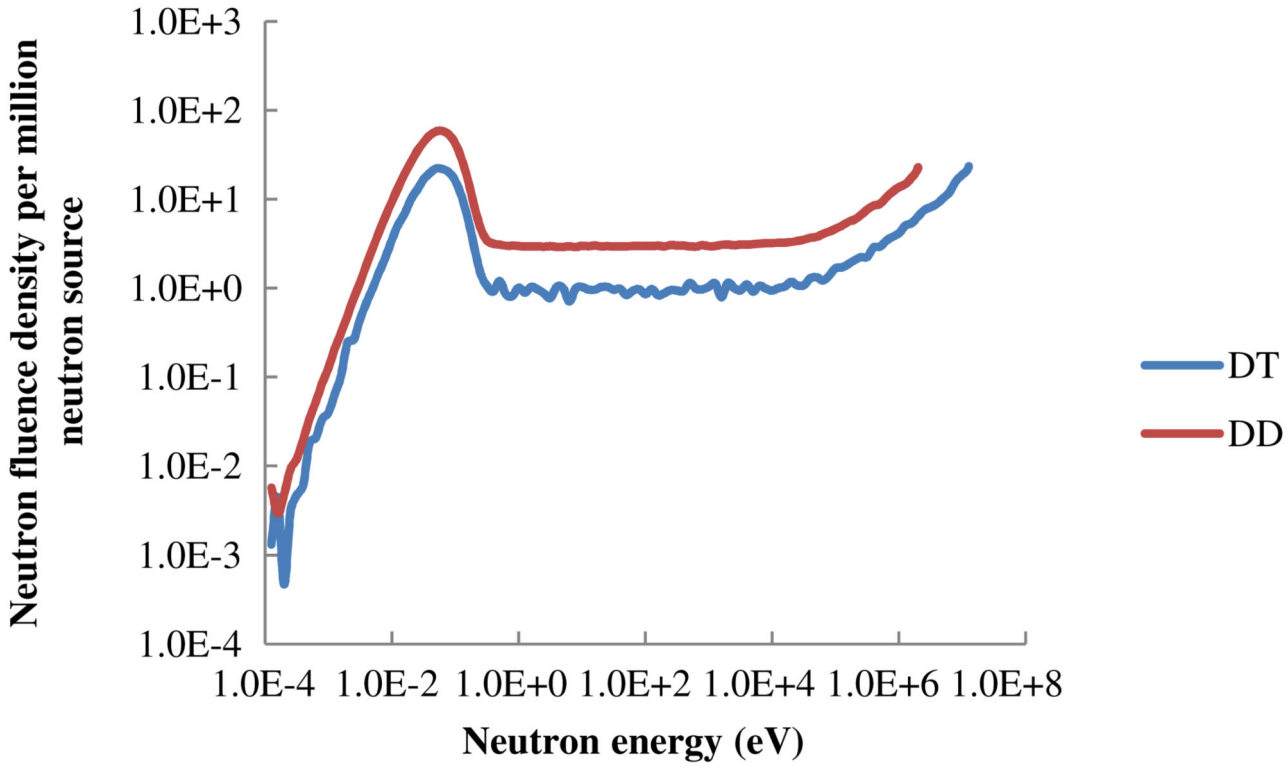

Figure 11.
DD and DT neutron fluences.

Table 1

Mass of each element and compound used in the hand phantoms.

	Ca	Cl	Na	Mg	Mn
Reaction	$^{48}Ca(n, \gamma)^{49}Ca$	$^{37}Cl(n, \gamma)^{38}Cl$	$^{23}Na(n, \gamma)^{24}Na$	$^{26}Mg(n, \gamma)^{27}Mg$	$^{55}Mn(n, \gamma)^{56}Mn$
Mass	13.925 g	1.205 g	1.29 g	242 mg	30, 150, 500 ppm
Compound added	$Ca_3(NO_3)_2\ 4H_2O$	NH_4Cl	$NaNO_3$	$Mg(NO_3)_2\ 6H_2O$	$Mn(NO_3)_2$
Mass	27.3 g	1.82 g	4.77 g	2.58 g	6.71, 33.55, 111.83 mg

Table 2

Neutron fluences at thermal and fast ranges for different moderators, including paraffin.

Moderator	Neutron fluence density per million neutron source at the thermal range	Neutron fluence density per million neutron source at the fast range
D_2O	7.34	245
H_2O	19.3	223
Graphite	9.21	248
Polyethylene	72.5	209
Paraffin	154	132

Table 3

Neutron fluences at thermal and fast ranges for different reflectors, including paraffin.

Reflector	Neutron fluence density per million neutron source at the thermal range	Neutron fluence density per million neutron source at the fast range
Al	186	154
Pb	254	162
Graphite	293	168
Polyethylene	333	147
Paraffin	373	140

Table 4

Neutron fluences at thermal and fast ranges for different thicknesses of paraffin moderator.

Thickness of the paraffin moderator (cm)	Neutron fluence density per million neutron source at the thermal range	Neutron fluence density per million neutron source at the fast range
2	42.1	225
3	49.6	156
4	52.4	107
5	51.9	76.9
6	49.7	54.4
7	45.7	38.7
8	39.9	27.1